Optics Communications 525 (2022) 128856

Contents lists available at ScienceDirect

Optics Communications

journal homepage: www.elsevier.com/locate/optcom

Theoretical analysis of optical bistability in a CW-pumped erbium-doped fiber laser

Juan Carlos Martín

Applied Physics Department-I3A, University of Zaragoza, 50009 Zaragoza, Spain

ARTICLE INFO

Keywords:
Erbium-doped fiber
Fiber laser
All-optical devices
Optical bistability

ABSTRACT

A theoretical model that allows numerical simulations of optical bistability phenomena in CW-pumped erbium-doped fiber lasers is presented. Results of the simulations match correctly with previous experimental data. In order to simulate this phenomenon, the population inversion and optical powers longitudinal distributions along the active fiber have been considered. If this fiber is long enough, it has been found that the transition between the non-lasing and the lasing states involves a dramatic redistribution of the population inversion along the active medium. This fact makes that non-lasing and lasing states constitute different enough initial conditions which determine different final responses to the same control parameter, that is to say, bistability. On the other hand, a theoretical justification is found for a previous experimental result which pointed out that the bistability range becomes reduced if an external signal is launched to the cavity. Finally, the bistability range width dependence on the active fiber length is analyzed.

1. Introduction

The study of bistability in lasers has attracted great interest due to its potential for the development of all-optical applications such as memory elements, switches or transistors [1–14]. In particular, erbium-doped fiber lasers (EDFL) provide an attractive basis for all-optical designs of these devices [7–17]. Bistability in EDFL has been obtained by means of different schemes. For sine-wave modulated pump, several nonlinear dynamical phenomena can be found: the temporal profile of the dynamic response controlled by the modulation frequency or the modulation index exhibits bistable behavior [9,10]. Bistability can also be achieved with modulation of the cavity losses [11] or with fixed modulation frequency and an external signal whose power is employed as control magnitude [12]. On the other hand, bistable behavior has also been reported making use of CW pump power as control magnitude [13–15]. In this case, an external signal can also be injected into the laser cavity and its effect is a modification in the bistability range width [16,17]. A recent experimental study can be found in [18] in which the link between bistability and saturable absorption in EDFL is shown.

Understanding of these phenomena are complete if a mathematical model which reproduces them is available. For sine-wave modulated pump, the bistable behavior observed was satisfactorily modeled by means of a nonautonomous system consisting of two ordinary differential equations [10]. Nevertheless, if CW pump power is considered, this model does not give rise to nonlinear responses [19,20]. Therefore, another model is necessary to account for bistability with CW pump power as control magnitude. Numerical results are provided in [16,17], with good agreement with the experimental results, but the details of the model employed were not explained there. The first aim of this work is providing a comprehensive presentation of the model employed in this comparison. Essentially, it deals with a conventional model in which the optical powers and population inversion distribution along the active fiber are taken into account.

In addition, it will be shown that, for long enough active fibers, the transition between non-lasing and lasing regime involves a dramatic population inversion redistribution along the active fiber. As it will be explained, this fact is the key for this bistability phenomenon and it justifies clearly the reason why a long enough active medium is necessary in order to obtain this effect. On the other hand, the external signal effect on the EDFL bistability range width is also explained with the basis of the mentioned population inversion redistribution.

The details of the model are provided in Section 2. Section 3 is devoted to the analysis of different EDFL responses calculated by means of the model, for various working conditions, which help to a deeper understanding of the bistability phenomenon studied here.

2. Model

Amongst the different possible EDFL configurations, the one considered for this work is shown in Fig. 1. The cavity consists of a ring containing the erbium-doped fiber (EDF) as active medium, with receives the input pump power thanks to a WDM and, optionally, also an input external signal or “control signal”, by means of coupler 1. According to the arrangement of the WDM and the coupler 1 ports,

E-mail address: jcmartin@unizar.es.

https://doi.org/10.1016/j.optcom.2022.128856
Received 9 June 2022; Received in revised form 30 July 2022; Accepted 2 August 2022
Available online 5 August 2022

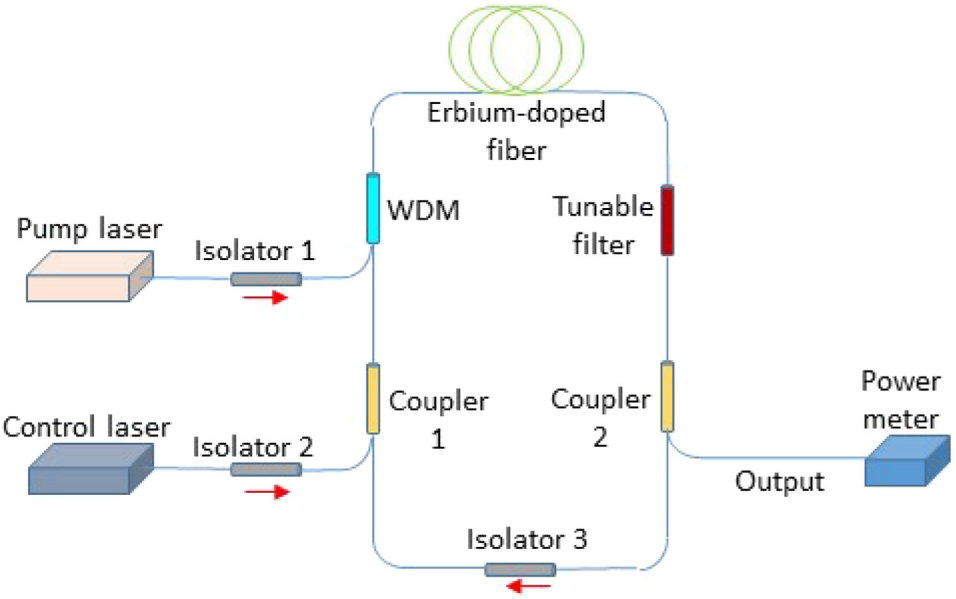

Fig. 1. Scheme of the ring laser considered.

together with the orientation of isolator 3, pump, laser and external signal lights coincide in their propagation senses. The tunable filter allows selection of the laser wavelength. Finally, coupler 2 is necessary to provide the laser output, whose power can be monitored by means of a power meter.

These EDFLs are frequently modeled by means of a simplified model in which ASE is neglected and pump power, laser power and the population distribution are averaged along the EDF [20,21]. Obviously, the shorter the EDF, the better the approximation. This model has been successfully employed to treat the EDFL transient behavior after pump power switch on [20,21] and the nonlinear response if a sine-wave modulated pump power is launched [10]. Nevertheless, if CW input pump power is considered, this model provides a linear equation relating pump and output laser powers [20], so it cannot explain the hysteresis cycles reported in [13–17].

The model presented here (employed in [16,17]) consists of an adaptation of the one presented in [22], which takes into account that the optical powers and the Er^{3+} laser transition levels population depend on the position along the active fiber. The amplified spontaneous emission (ASE) effect on the system performance turns out to be negligible when the lasing regime takes place. Nevertheless, ASE is also included in the model in order to account for light power emission of the system even if it does not lase.

Propagation of the optical powers are ruled by equations similar to the ones employed for an erbium doped fiber amplifier [22]:

$$\frac{dP_p(z,t)}{dz} = P_p(z,t)\left\{\left[\gamma_a(\nu_p)+\gamma_e(\nu_p)\right]N(z,t)-\gamma_a(\nu_p)\right\} \quad (1)$$

$$\frac{dP_s(z,t)}{dz} = P_s(z,t)\left\{\left[\gamma_a(\nu_s)+\gamma_e(\nu_s)\right]N(z,t)-\gamma_a(\nu_s)\right\} \quad (2)$$

$$\frac{dP_f^{\pm}(z,\nu,t)}{dz} = \pm 2h\nu\Delta\nu\gamma_e(\nu)N(z,t) \pm P_f^{\pm}(z,\nu,t)(z,t)\left\{\left[\gamma_a(\nu)+\gamma_e(\nu)\right]N(z,t)-\gamma_a(\nu)\right\} \quad (3)$$

In these equations, z is the longitudinal coordinate along the EDF and t is the temporal coordinate. The first two equations account for propagation of pump and external signal powers, P_p and P_s, whose central optical frequencies are ν_p and ν_s, respectively. Implicitly, these equations establish that the propagation direction of both pump and signal is the positive one along the z axis. The third equation accounts for ASE propagation. In order to treat it, its spectrum is discretized in channels whose central frequency and bandwidth are ν and $\Delta\nu$, respectively. P_f^+ and P_f^- denote ASE power at a certain channel propagating in positive and negative directions, respectively, and h is the Planck constant. In the three equations, γ_a and γ_e represent absorption and emission coefficients and N stands for the ratio between the population of the Er^{3+} laser transition upper level ($^4I_{13/2}$) and the Er^{3+} concentration. Its evolution is ruled by next equation:

$$\frac{dN(z,t)}{dt} = W_a(z,t) - \left[W_a(z,t)+W_e(z,t)+\frac{1}{\tau}\right]N(z,t), \quad (4)$$

in which τ is the laser transition upper level lifetime and W_i $(i = a, e)$ is:

$$W_i(z,t) = \frac{1}{hN_T}\left\{\frac{P_p(z,t)\gamma_i(\nu_p)}{\nu_p}+\frac{P_s(z,t)\gamma_i(\nu_s)}{\nu_s} + \sum_{\nu}\frac{\left[P_f^+(z,\nu,t)+P_f^-(z,\nu,t)\right]\gamma_i(\nu)}{\nu}\right\}, \quad (5)$$

where N_T is the number of Er^{3+} ions per EDF unit length.

Note that in [22] also overlapping factors are included in the equations. It has been checked that the quantitative difference in the results presented here, either considering overlapping factors or not, is less than 3%. Besides, it will be shown that they are not necessary in order to model the phenomenon qualitatively. For these reasons, overlapping factors have not been included in the model employed here.

In order to model a setup as shown in Fig. 1, it is assumed that the tunable filter allows transmission of only one fluorescence channel, corresponding to the optical frequency ν_l (always chosen different from ν_s). Besides, isolator 3 only allows propagation in the positive direction. Therefore, the only power that propagates all around the ring is P_f^+ at the ν_l channel, called P_l from now on. In order to relate P_l values at the EDF ends, $z = 0$ and z = L, the following condition is imposed [22]:

$$P_l(0,t_i+\Delta t) = T\,P_l(L,t_i), \quad (6)$$

where T is the ring transmission factor at $\nu = \nu_l$, save for the EDF, Δt is the one round trip time, employed here as temporal step for numerical calculations, and $t_i = i\Delta t$ $(i = 0, 1, 2,\ldots)$. In lasing regime, $P_l(z, t)$ represents the laser power distribution along the EDF. On the other hand, the laser output power is $P_{out}(t) = aP_l(L, t)$, a being the power fraction transmitted by the tunable filter and led to the output port by means of coupler 2 (Fig. 1).

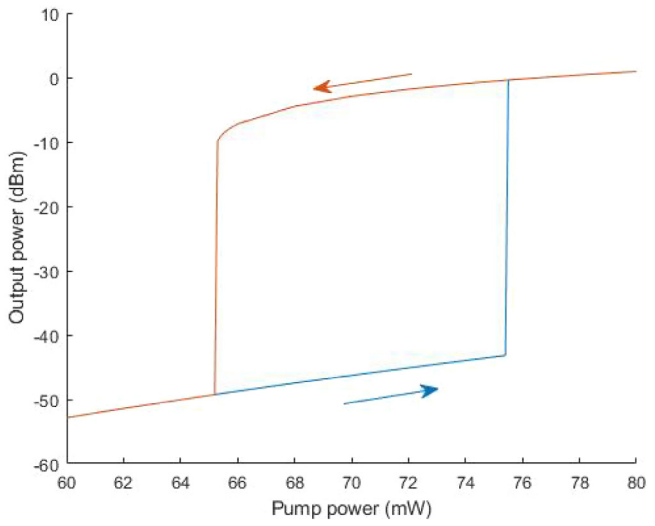

Fig. 2. Hysteresis cycle without external signal. Blue: response for pump power ascending sweep at the bistability range; yellow: response for pump power descending sweep or for pump power outside the bistability range.

3. Results

The bistability experiments reported in [16,17] consist of registering the output laser power as a function of a series of input pump power values $P_{p,in}^{(j)}$ (j = 1,2,... n) that is followed first in ascending order and then in descending order. The numerical procedure to simulate this experiment has been the following. At $t = 0$, the initial condition N(z, 0) = 0 is established. From $t = 0$ on, $P_s(0, t)$ takes a fixed value along the whole calculation and $P_p(0, t) = P_{p,in}^{(1)}$. The transient ring response is calculated until the steady state is reached, and the laser output power $P_{out}^{(1)}$ is registered. Next, $P_p(0, t) = P_{p,in}^{(2)}$ and the subsequent transient response is calculated, with the final N(z) distribution of the previous steady state as initial distribution for this second transient. Its steady state output power is registered as $P_{out}^{(2)}$. The ascending series is completed by iterating until $j = n$ and, the same way, the descending series is obtained by calculating the transient with $P_{p,in}^{(n-1)}$ departing from the steady state reached with $P_{p,in}^{(n)}$, then the transient with $P_{p,in}^{(n-2)}$ departing from the steady state reached with $P_{p,in}^{(n-1)}$ and so on, until $j = 1$. Fig. 2 shows the result of a series, calculated without external input signal and with the following parameters: pump at 980 nm wavelength, with $\gamma_a(\nu_p) = 4.37$ dB/m and, as usually assumed for Er^{3+} at this wavelength, $\gamma_e(\nu_p) = 0$; third window γ_a and γ_e spectra as shown in [16]; ring laser wavelength: 1550 nm, so that, according to [16], $\gamma_a(\nu_l) = 2.31$ dB/m and $\gamma_e(\nu_l) = 3.21$ dB/m; $T = 0.11$; $L = 30$ m; ring optical path: 58.8 m; $\tau = 10.5$ ms; $N_T = 2.3\ 10^{14}$ m^{-1}; $a = 0.1$. Pump power is increased or decreased at 0.1 mW steps. This series is similar to the one employed in [16]. It is worthwhile to remark that the upper branch corresponds to emission in laser regime, while the lower branch represents the system states in which the lasing condition does not meet.

For later discussions, it is convenient to establish some terminology. In ascending sweep, the first pump power value which makes the system lase will be called here "ascending critical pump power". The same way, in descending sweep, the last pump power value which makes the system lase will be called here "descending critical pump power". The difference between both values will be referred to as "bistable range width".

Fig. 3 shows several N(z) distributions for steady states corresponding to different pump powers belonging either to the ascending or descending series (Figs. 3A and 3B, respectively). Profiles corresponding to the lower branch at Fig. 2 (non-lasing regime) and upper branch (lasing regime) are plotted with dashed line and solid line, respectively, for several input pump powers specified at the upper right insets.

In order to describe qualitatively several features of the curves obtained, the EDF can be divided into three regions: left (z < 10 m), middle (10 m < z < 20 m) and right (z > 20 m) (the limits are only rough references). On the other hand, with the $\gamma_a(\nu_l)$ and $\gamma_e(\nu_l)$ values considered, the gain condition at the laser frequency is $N > 0.41$. Therefore, in lasing regime the middle and left regions turn out to be absorbing (with the approach employed in [18], this distribution corresponds to saturable absorption). Remark that, in the EDFLs usually considered in the Literature, active fiber lengths are shorter in order to avoid the presence of absorbing regions, face to maximize the device output power (an example of it is Ref. [22], whose N(z) figures may be interesting to compare with Fig. 3). In contrast, the case analyzed here corresponds to what will be called here "overlong laser", or laser whose active medium presents a wide absorbing region in lasing regime. Fig. 3 offers not only a specific interest due to its direct link to the bistability phenomenon under study, but also an interest from the general point of view of laser theory, as it shows peculiar properties of N(z) distributions in overlong lasers still not reported to my knowledge.

With regard to bistability, the most significant feature in Fig. 3 is the pronounced N(z) profile difference between non-lasing and lasing regime curves: the former present a softly rounded plateau at the left region, a steep decay in the middle region and a much softer decay in the right region; in contrast, the latter's left region presents a steep decay, while in the middle and right regions the N(z) decay is much slower. The sharp N(z) redistribution associated to the change of regime is key for the bistability observed: it is well-known that, in any bistable system, the final system response to a variation in the control parameter value is conditioned by the system initial state, defined in EDFLs by its initial N(z) distribution. The more different the initial states are, the greater the chance they influence the final state and, consequently, the more likely the occurrence of bistability. The overlong EDF length is the key for the appearance of remarkable N(z) differences between non-lasing and lasing regime, and, therefore, the key for bistability in an EDFL.

On the other hand, a short digression is worthwhile in order to remark some other overlong laser peculiarities not directly linked with bistability. Remind that in a simple CW-pumped laser model, the active medium state is characterized by a single upper laser level population value which increases with pump power in non-lasing regime and remains constant in lasing regime, so that gain provided by the active medium equals the cavity losses. Nevertheless, in Fig. 3 both regimes present some more details: in non-lasing regime, the average N(z) increase with pump power happens mainly due to an enlargement of the left region plateau without a remarkable height increase, together with softening the decays in the middle and right regions (the opposite also holds for pump power decrease); and in lasing regime, the N(z) profile does change as pump power is varied (without changing the gain provided by the whole active medium, which of course equals the cavity losses).

The transition from non-lasing to lasing regime can be analyzed with greater detail. For the case shown in Fig. 2, the ascending critical pump power is 75.5 mW. More specifically, the transition happens during the transient after the pump power switch from 75.4 mW to 75.5 mW ($t = 0$ from now on). Fig. 4 shows the laser output power during this transient. It can be seen that the build-up time or time corresponding to the first laser spike is 33.10 ms. Fig. 5 shows how the N(z) distribution evolves in the vicinity of the build-up time. Before the first spike appearance, changes in N(z, t) along time are less than 0.5% for any z. For this reason, only one N(z) distribution before the first spike has been plotted (dashed blue line). Fig. 5A shows different N(z) distributions along 1 ms comprising the first spike instant, in which a clear evolution can be appreciated. Fig. 5B shows N(z) distributions along nearly 7 ms. It can be appreciated that the steady state distribution has almost been achieved at $t = 39.22$ ms (according to Fig. 4, it

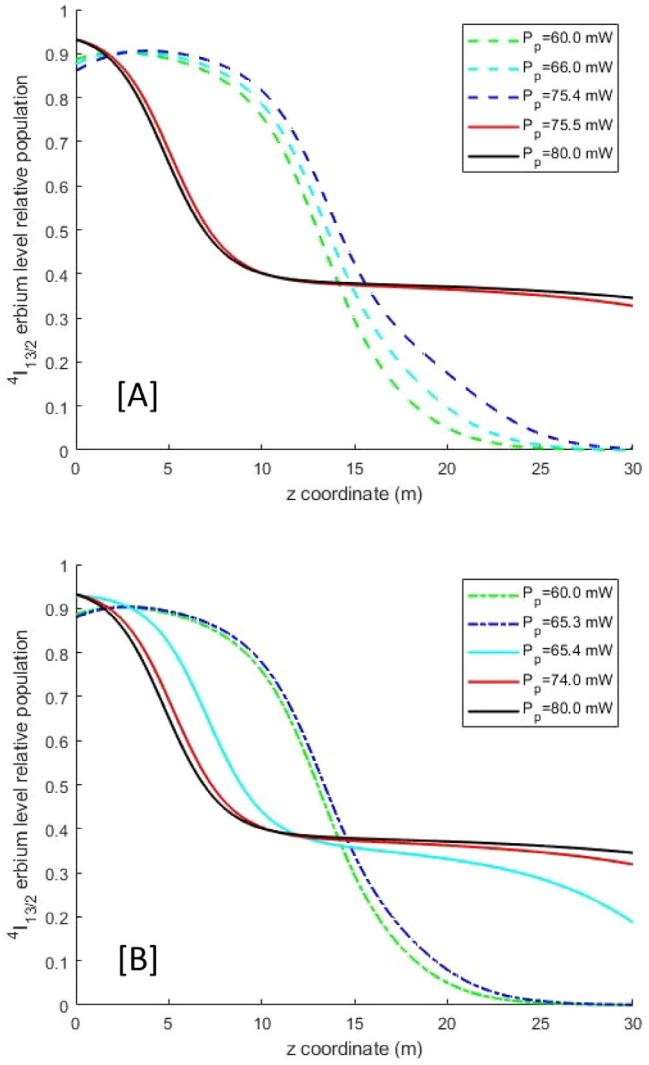

Fig. 3. N(z) distributions along the EDF in the laser considered, for different CW pump powers either if their values are swept in ascending [A] or descending [B] order. No external signal power is coupled. Dashed lines correspond to non-lasing regime. Solid lines correspond to lasing regime.

can be accepted that at t = 100 ms the system has reached its steady state). So, in this case, around 7 ms are enough to complete most of the N(z) redistribution process.

The same way, it is also convenient to show the details of the transition from lasing to non-lasing regime in the descending sweep (pump power switch from 65.4 mW to 65.3 mW): Fig. 6 shows the laser output power during the transient and Fig. 7 shows N(z) distributions at several time instants. Obviously, there are plain differences between the ascending and descending transitions and in no way can one be considered the reverse of the other. It is interesting to remark that most of the N(z) readjustment takes place after t = 16.5 ms, when the laser output apparently vanishes (Fig. 6) (in fact it decreases around 40 dB, Fig. 2).

In view of the results obtained, it is worthwhile to remark that the cause of the phenomenon under study can be attributed to a nonlinear dynamical behavior: the system under study could appear to be static as we talk about CW pump, but in fact any change in the CW pump power induces a time-dependent, dynamical response which has been shown to be key for the explanation of the hysteresis cycles obtained.

As reported in [16,17], launching an external signal in Fig. 1 setup narrows the system bistability range. Fig. 8 shows the example

Table 1
D_{asc}, D_{des}, and D parameters (all of them defined in the text) for the transitions represented in Figs. 2 and 8.

	D_{asc}	D_{des}	D
No external signal (Fig. 2)	0.231	0.188	0.210
With external signal (Fig. 8)	0.161	0.138	0.149

corresponding to an external signal power of 0.2 mW at a wavelength of 1520 nm (a similar series is shown in [17]). According to the spectrum shown in [17], $\gamma_a(\nu_s)$ = 3.39 dB/m and $\gamma_e(\nu_s)$ = 2.52 dB/m. The main difference with regard to Fig. 2 is the ascending critical pump power: 68.1 mW with the mentioned external signal (Fig. 8) and 75.4 mW in absence of external signal (Fig. 2). On the other hand, the opposite transition has much closer critical pump powers: 65.4 mW (Fig. 2) and 64.7 mW (Fig. 8).

Fig. 9 shows various N(z) profiles corresponding to several system states represented in Fig. 8. It is worthwhile to compare these profiles with distributions in absence of external signal (Fig. 3). Differences between both figures' N(z) distributions are more evident in non-lasing than in lasing regime. Non-lasing regime N(z) profiles in Fig. 9 exhibit narrower left plateaus compared with non-lasing regime N(z) profiles in Fig. 3, together with a more gradual decay in the center and right regions. The profile modification induced by the external signal may justify the bistability range width reduction if an external signal is added [16,17]: as a rule of thumb, it may be conjectured that the closer the N(z) profiles corresponding to both branches in the vicinity of a transition, the easier the shift between branches, which favors a narrower hysteresis cycle. The difference between N(z) profiles in the vicinity of a transition can be quantified by means of the following parameter:

$$D_\alpha = \frac{1}{L}\int_{z=0}^{L} \left|N_b(z) - N_a(z)\right| dz, \tag{7}$$

where N_b(z) and N_a(z) correspond respectively to the states before and after the critical pump step which induces the transition (for instance, for characterization of the ascending sweep transition in Fig. 8, N_b and N_a are the profiles in Fig. 9A corresponding to 68.0 and 68.1 mW pump powers, respectively). The subscript α may be "asc" or "des", specifying whether the transition happens for ascending or descending pump sweep. Table 1 presents the D_{asc} and D_{des} parameters corresponding to the transitions shown in Figs. 2 and 8. The parameters corresponding to the former are greater than the ones corresponding to the latter. In agreement with the rule of thumb proposed, the bistability range in Fig. 2 is greater than in Fig. 8.

Both D_{asc} and D_{des} provide an idea about the difference between the branches corresponding to lasing and non-lasing regimes, but in order to characterize such difference by a single parameter, the average between D_{asc} and D_{des} will be considered:

$$D = \frac{1}{2}\left(D_{asc} + D_{des}\right). \tag{8}$$

Finally, it is interesting to analyze the bistability range dependence on the EDF length. Fig. 10A shows the ascending and descending critical pump powers (that is to say, the bistability range limits), in absence of external signal, as a function of the EDF length (the rest of the ring elements remain the same, so each EDF length modification makes the ring optical path change accordingly). It is clear that the bistability appears for long enough EDF length. In the cases analyzed, L = 20 m is the lower length in which bistability is observed, with a 0.1 mW range width. Besides, the longer the EDF length, the wider the bistability range. On the other hand, Fig. 10B shows the D parameter dependence on the EDF length. This result means that the difference between N(z) distributions characteristic of non-lasing and lasing states becomes intensified as the EDF length increases. In particular, this idea explains the reason why a bistable EDFL requires an overlong EDF: it may be interpreted that only if L is long enough, such difference is pronounced enough to give rise to bistability.

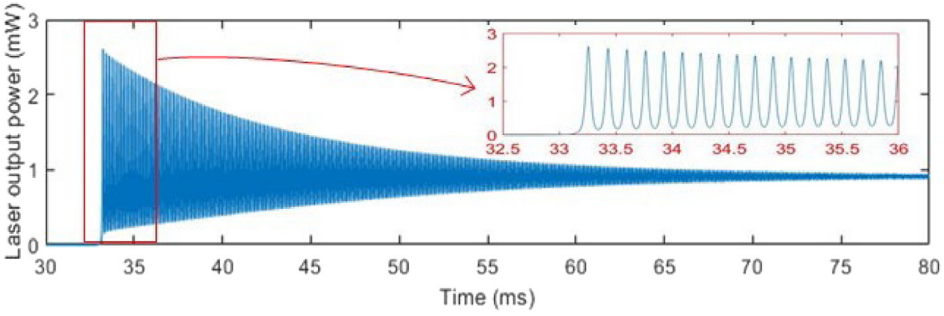

Fig. 4. Laser output power during the transient after input pump power switch from P_p = 75.4 mW to P_p = 75.5 mW (t = 0). The inset shows the detail of the first spikes.

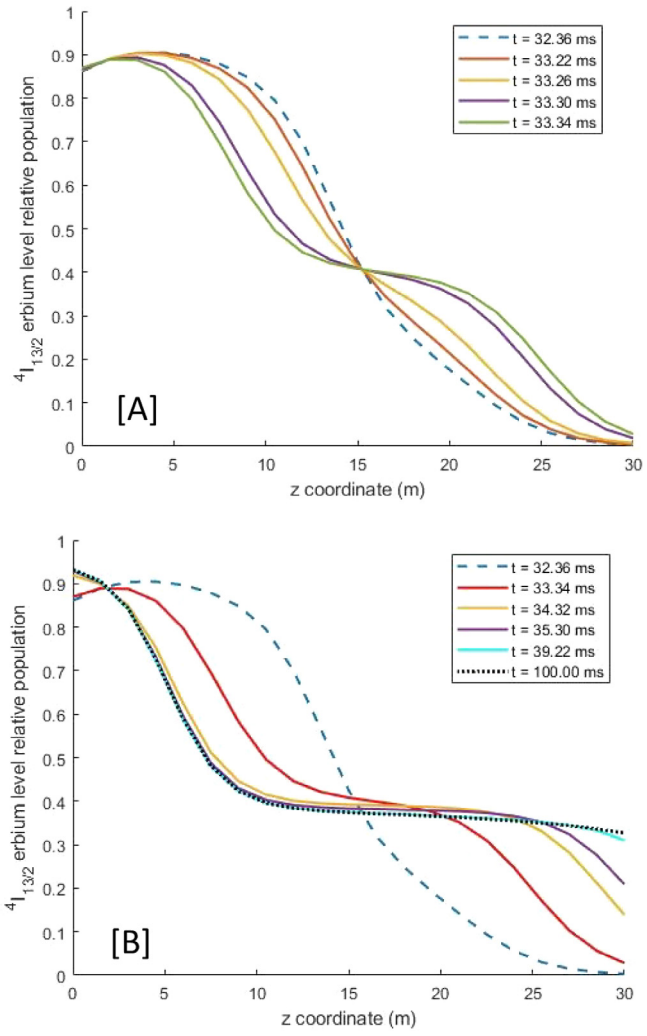

Fig. 5. N(z) distributions along the EDF in the laser considered, for different time instants during the laser transient shown in Fig. 4. [A]- N(z) variation during 0.98 ms. [B]-N(z) variations during 6.86 ms and comparison with the N(z) distribution at t = 100 ms (dotted line). In dashed line, the only N(z) distribution plotted, corresponding to an instant previous to the first laser spike.

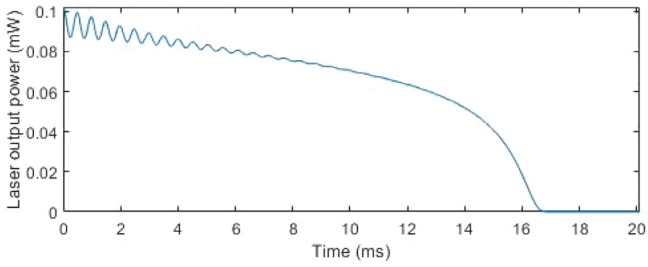

Fig. 6. Laser output power during the transient after input pump power switch from P_p = 65.4 mW to P_p = 65.3 mW (t = 0).

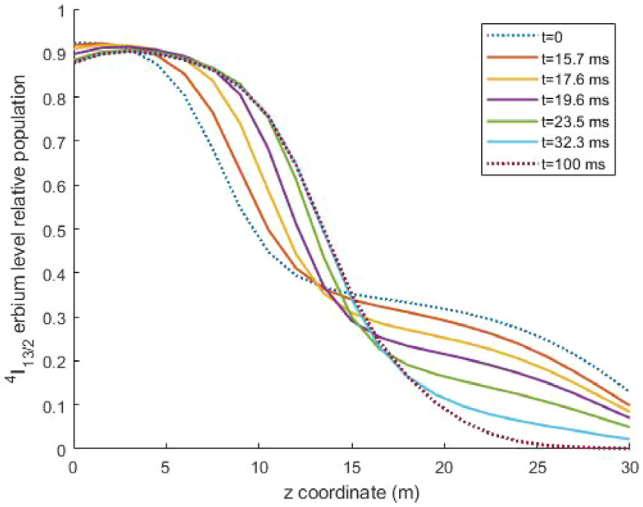

Fig. 7. N(z) distributions along the EDF in the laser considered, for different time instants during the laser transient whose first 20 ms are shown in Fig. 6.

4. Conclusions

The cause of the bistability phenomenon observed in EDFLs with CW pump power as control parameter has been explained: it can be attributed to a nonlinear dynamical behavior found during the transient between pump power value shifts. A numerical model which reproduces correctly the experimental results previously observed has been detailed. In addition, this model allows one to determine N(z), the upper laser level transition population distribution along the active medium. A sharp difference between N(z) distributions in non-lasing and lasing regime has been found in overlong EDFLs. Thanks to it, non-lasing and lasing states constitute "different enough" initial conditions to make bistability possible.

A parameter, D, has been proposed to quantify the difference between initial conditions. It is shown that the presence of an external signal diminishes such difference, which justifies the bistability width reduction observed if some external signal is launched. On the other hand, it is shown that D increases with the EDF length, which explains the need for overlong lasers in order to observe this bistability phenomenon.

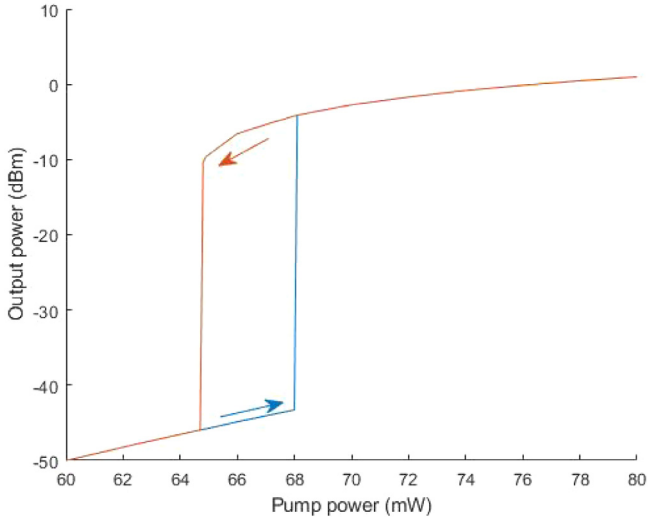

Fig. 8. Hysteresis cycle with external signal whose power and wavelength are 0.2 mW and 1520 nm, respectively. Blue: response for pump power ascending sweep at the bistability region; yellow: response for pump power descending sweep or for pump power outside the bistability range.

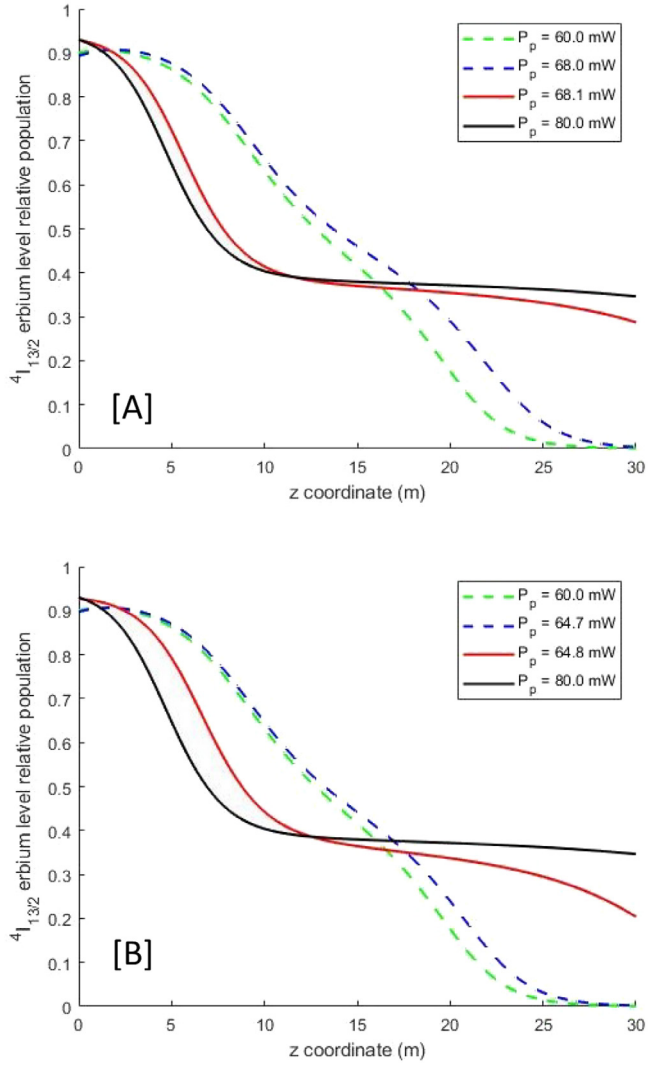

Fig. 9. N(z) distributions along the EDF in the laser considered, for different CW pump powers either if their values are swept in ascending [A] or descending [B] order. External signal power and wavelength: 0.2 mW and 1520 nm, respectively. Dashed lines correspond to non-lasing regime. Solid lines correspond to lasing regime.

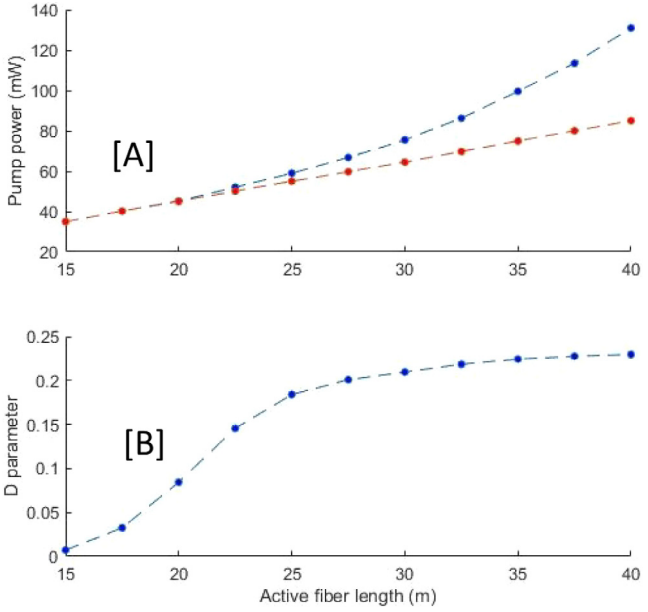

Fig. 10. [A] Critical pump power for ascending (blue) and descending (orange) pump sweep, as a function of the EDF length, in absence of external signal. [B] Corresponding D parameter.

Declaration of competing interest

The authors declare that they have no known competing financial interests or personal relationships that could have appeared to influence the work reported in this paper.

Data availability

Data will be made available on request.

Acknowledgments

This work has been sponsored by the Department of Industry and Innovation (Gobierno de Aragón) through the research group Grant E44_20R (cofunded with Feder 2014-2020: Building Europe from Aragon).

References

[1] C.H. Chen, S. Matsuo, K. Nozaki, A. Shinya, T. Sato, Y. Kawaguchi, H. Sumikura, M. Notomi, Opt. Express 19 (2011) 3395–3397.
[2] K. Huybrechts, G. Morthier, R. Baets, Opt. Express 16 (2008) 11405–11410.
[3] T. Perez, A. Scire, G. Van der Sande, P. Colet, C.R. Mirasso, Opt. Express 15 (2007) 12941–12948.
[4] Q.H. Mao, J. Lit, I.E.E.E. Photon. Technol. Lett. 14 (2002) 1252–1254.
[5] H.M. Gibbs, Optical Bistability: Controlling Light with Light, Academic, New York, 1985.
[6] Z.P. Wang, B.L. Yu, J. Opt. Soc. Amer. B 30 (2013) 2915–2920.
[7] F. Sanchez, G. Stephan, Phys. Rev. E 53 (1996) 2110–2122.
[8] Z.P. Wang, B.L. Yu, J. Appl. Phys. 113 (2013) 113101.
[9] L.G. Luo, T.J. Tee, P.L. Chu, Opt. Commun. 146 (1998) 151–157.
[10] I.J. Sola, J.C. Martín, J.M. Álvarez, Opt. Commun. 212 (2002) 359–369.
[11] J.M. Saucedo-Solorio, A.N. Pisarchik, A.V. Kir'yanov, V. Aboites, J. Opt. Soc. Amer. B 20 (2003) 490–496.
[12] J.C. Martín, IEEE Photon. Tech. Lett. 292-294 (2016) 1973–1975.
[13] J.M. Oh, D. Lee, IEEE J. Quantum Electron. 40 (2004) 374–377.
[14] Q. Mao, S. Feng, W. Liu, W.Y. Lit, IEEE Photon. Tech. Lett. 18 (2006) 1973–1975.
[15] J. Shao, S. Li, Q. Shen, Z. Wu, Z. Cao, J. Gu, Opt. Express 15 (2007) 3673–3679.
[16] Q. Ge, S. Li, Z. Wang, S. Zhen, J.C. Martín, B. Yu, Opt. Laser. Technol. 98 (2018) 79–83.
[17] S.L. Li, Q. Ge, Z.P. Wang, J.C. Martín, B.L. Yu, Sci. Rep. 7 (2017) 8992.
[18] D. Jachpure, R. Vijaya, J. Opt. 24 (2022) 024007.
[19] S.H. Strogatz, Nonlinear Dynamics and Chaos, Perseus Publishing, New York, 1994.
[20] I.J. Sola, J.C. Martín, J.M. Álvarez, S. Jarabo, Opt. Commun. 193 (2001) 133–140.
[21] O.G. Okhotnikov, V.V. Kuzmin, J.R. and Salcedo, IEEE Photon. Technol. Lett. 6 (1994) 362–364.
[22] I.J. Sola, J.C. Martín, J.M. Álvarez, J. Modern Opt. 53 (2006) 525–538.